

Electric dipole moments from the perspective of a scalar triplet and singlet extension of the MSSM: A study of neutrons, electrons, mercury, and b and c quarks

Qing-hua Li^{1,2*}, Jin-Lei Yang^{1,2,3†}, Xiang Yang^{1,2,3‡}, Tai-Fu Feng^{1,2,3,4§}

¹ *Department of Physics, Hebei University, Baoding 071002, China*

² *Hebei Key Laboratory of High-precision Computation and Application of Quantum Field Theory, Baoding, 071002, China*

³ *Hebei Research Center of the Basic Discipline for Computational Physics, Baoding, 071002, China and*

⁴ *Department of Physics, Chongqing University, Chongqing 401331, China*

(Dated: February 6, 2025)

Abstract

In the framework of the minimal supersymmetric model extension with new scalar triplets and singlet (TNMSSM), we analyze the electric dipole moment (EDM) of neutron (d_n), electron EDM(d_e), the mercury EDM(d_{Hg}), b quark (d_b) and c quark (d_c) by considering the contributions from the one-loop diagrams, some two-loop diagrams and the Weinberg operators. The effects of TNMSSM specific CPV sources χ_d , χ_t on d_n , d_e , d_{Hg} , d_b , d_c are specialized, it is found that they have significant contributions to these EDMs, and the current upper bounds on d_n impose strict constraints on χ_d , χ_t . The theoretical predictions on d_b , d_c can reach about 10^{-22} e-cm and 10^{-23} e-cm respectively by taking the upper bounds on d_n , d_e , d_{Hg} into account, which have great potential to be observed in future.

PACS numbers:

Keywords: CP violating, neutron, electric dipole moment

* lqhlqh202408.163.com

† jlyang@hbu.edu.cn

‡ yangxiang202406@163.com

§ fengtf@hbu.edu.cn

I. INTRODUCTION

In the early universe, the interaction of high-energy particles would lead to the symmetric production of matter and antimatter. However, the observations of baryon asymmetry in the current universe indicate this symmetry was broken under some mechanism [1]. This mechanism requires more CP-violating (CPV) sources beyond the standard model (SM) [2, 3], because the sole sources of CPV in the SM are the Cabbibo-Kobayashi-Maskawa (CKM) phases at quark sector, and the computational results indicate that the produced values are too small to adequately account for the observed asymmetry between matter and antimatter [4–6]. The introducing of new CPV phases may make significant contributions to the electric dipole moments (EDMs) of particles, while these EDMs are highly suppressed in the SM [7]. Hence, the observations of the EDMs can provide clear signals of CPV effects in NP [8–12].

In this work, we focus on the EDMs of neutron (d_n), electron EDM(d_e), the mercury EDM(d_{Hg}), b quark (d_b) and c quark (d_c) in the framework of the minimal supersymmetric model (MSSM) extension with new scalar triplets and singlet (TNMSSM) [13–15]. Although d_n , d_e , d_{Hg} , d_b , d_c are not observed experimentally so far, strict upper bounds on them have been obtained [16–22]

$$\begin{aligned}
 |d_n| &< 1.8 \times 10^{-26} \text{e} \cdot \text{cm}, \\
 |d_e| &< 4.1 \times 10^{-30} \text{e} \cdot \text{cm}, \\
 |d_{Hg}| &< 7.4 \times 10^{-30} \text{e} \cdot \text{cm}, \\
 |d_b| &< 2.0 \times 10^{-17} \text{e} \cdot \text{cm}, \\
 |d_c| &< 4.4 \times 10^{-17} \text{e} \cdot \text{cm}.
 \end{aligned} \tag{1}$$

In addition, the chromoelectric dipole moments (CEDM) of heavy quarks is tightly constrained by the upper bound on d_n , which can be expressed as [23]

$$d_n = (1 \pm 0.5)[1.4(d_d^\gamma - 0.25d_u^\gamma) + 1.1e(d_d^g + 0.5d_u^g)] \pm (22 \pm 10) \text{MeV}C_5, \tag{2}$$

d_q^γ , d_q^g , C_5 represent the EDM of quark q from the electroweak interaction, CEDM of quark q and the coefficient of the Weinberg operator at the chirality scale, respectively. Using the

running from Refs. [24, 25], $d_{d,u}^{\prime g}$ and C_5 can be expressed in the form of d_c^g at the m_c scale [22]. Subsequently, a new upper limit $|d_c^g| < 1.0 \times 10^{-22} \text{cm}$ can be obtained by considering the limits on d_n . Through the calculation of the rigorous constraints on d_b^g in Refs. [22, 26, 27], a new limits for the EDMs of b and c quarks can be derived

$$\begin{aligned} |d_b| &< 1.2 \times 10^{-20} \text{e} \cdot \text{cm}, \\ |d_c| &< 1.5 \times 10^{-21} \text{e} \cdot \text{cm}. \end{aligned} \tag{3}$$

The above results improve the previous bounds in Eq. (1) by about three orders of magnitude. It is obvious that the experimental upper limits on these quantities are strict, hence the contributions from new CPV phases in NP models may be tightly constrained, and researching NP effects on these EDMs may help to elucidate the mechanism of CPV [28, 29].

The TNMSSM extends the MSSM with two $SU(2)_L$ triplets and an additional scalar singlet [30]. The μ problem of the MSSM [31, 32] can be solved by introducing the scalar singlet in the TNMSSM, and μ is at about the electroweak scale naturally after the scalar singlet achieving nonzero vacuum expectation value (VEV) [33–35]. The μ term is the primary source of baryon asymmetry, and large phase of μ required by baryon asymmetry enhances the theoretical predictions on the EDMs d_n , d_b , d_c , d_e , d_{Hg} significantly. Similarly, mutual cancellations between different phases are most likely to suppress the EDM to below the corresponding experimental upper limits [36–43]. And the so-called little hierarchy problem can also be alleviated by introducing two scalar triplets. Correspondingly, there are also new CPV sources in the TNMSSM compared with the MSSM, hence we explore the effects of CPV sources in the TNMSSM on d_n , d_b , d_c , d_e , d_{Hg} in this work.

The paper is organized as follows. In Section II, the overview of the key elements of the TNMSSM are briefly summarized by introducing the superpotential and the general soft breaking terms. Then Section III analyzes the EDM of neutron d_n , b quark d_b , c quark d_c , electron EDM d_e and mercury EDM d_{Hg} . In order to see the corrections to these EDMs clearly, the numerical results of d_n , d_b , d_c , d_e , d_{Hg} with new CPV phases are explored in Section IV. Conclusions are summarized in Section V.

II. THE TNMSSM

Besides the superfields \hat{H}_d, \hat{H}_u of the MSSM, TNMSSM introduces a gauge singlet superfield S and two $SU(2)_L$ triplet superfields T and \bar{T} [13, 14]

$$\begin{aligned} \hat{T} &= \begin{pmatrix} \frac{1}{\sqrt{2}}T^+, & -T^{++} \\ T^0, & \frac{-1}{\sqrt{2}}T^+ \end{pmatrix} \sim (1, 3, 1), & \hat{\bar{T}} &= \begin{pmatrix} \frac{1}{\sqrt{2}}\bar{T}^-, & -\bar{T}^0 \\ \bar{T}^{--}, & \frac{-1}{\sqrt{2}}\bar{T}^- \end{pmatrix} \sim (-1, 3, 1), \\ \hat{H}_d &= \begin{pmatrix} H_d^0 \\ H_d^- \end{pmatrix} \sim (-1/2, 2, 1), & \hat{H}_u &= \begin{pmatrix} H_u^+ \\ H_u^0 \end{pmatrix} \sim (1/2, 2, 1), & \hat{S} &\sim (0, 1, 1). \end{aligned} \quad (4)$$

$T^+, \bar{T}^-, H_d^-, H_u^-$ are singly-charged Higgs, T^{++}, \bar{T}^{--} are doubly-charged Higgs, $H_d^0, H_u^0, T^0, \bar{T}^0, S$ are complex neutral superfields [44–46]

$$\begin{aligned} H_d^0 &= \frac{1}{\sqrt{2}}(v_d + \text{Re}H_d^0 + i\text{Im}H_d^0), & H_u^0 &= \frac{1}{\sqrt{2}}(v_u + \text{Re}H_u^0 + i\text{Im}H_u^0), \\ T^0 &= \frac{1}{\sqrt{2}}(v_T + \text{Re}T^0 + i\text{Im}T^0), & \bar{T}^0 &= \frac{1}{\sqrt{2}}(v_{\bar{T}} + \text{Re}\bar{T}^0 + i\text{Im}\bar{T}^0), \\ S &= \frac{1}{\sqrt{2}}(v_S + \text{Re}S + i\text{Im}S), \end{aligned} \quad (5)$$

where $v_d, v_u, v_T, v_{\bar{T}}$ and v_S are the corresponding VEVs.

The superpotential of the TNMSSM can be represented as [47]

$$\begin{aligned} W_{\text{TNMSSM}} &= Y_u \hat{U}^c \hat{H}_u \cdot \hat{Q} - Y_d \hat{D}^c \hat{H}_d \cdot \hat{Q} - Y_e \hat{E}^c \hat{H}_d \cdot \hat{L} + \chi_d \hat{H}_d \cdot \hat{T} \hat{H}_d \\ &\quad + \chi_u \hat{H}_u \cdot \hat{\bar{T}} \hat{H}_u + \frac{1}{3} \kappa \hat{S} \hat{S} \hat{S} + \lambda \hat{S} \hat{H}_u \cdot \hat{H}_d + \Lambda_T \hat{S} \text{Tr}(\hat{T} \hat{T}). \end{aligned} \quad (6)$$

The soft SUSY breaking terms are [48]

$$\begin{aligned} -\mathcal{L}_{\text{soft}} &= m_{H_u}^2 |H_u|^2 + m_{H_d}^2 |H_d|^2 + m_S^2 |S|^2 + m_T^2 \text{Tr}(|T|^2) + m_{\bar{T}}^2 \text{Tr}(|\bar{T}|^2) \\ &\quad + m_Q^2 |Q|^2 + m_u^2 |u|^2 + m_d^2 |d|^2 + (T_{\Lambda_T} S \text{Tr}(T \bar{T}) + T_\lambda S H_u \cdot H_d + \frac{1}{3} T_\kappa S^3 \\ &\quad - T_{\chi_u} H_u \cdot \bar{T} H_u - T_{\chi_d} H_d \cdot T H_d + T_{u,ij} \tilde{Q}_j \cdot H_u \tilde{u}_i^c - T_{d,ij} \tilde{Q}_j \cdot H_d \tilde{d}_i^c + H.c.), \end{aligned} \quad (7)$$

where [49]

$$\begin{aligned} H_u \cdot H_d &= H_u^+ H_d^- - H_u^0 H_d^0, \\ H_d \cdot T H_d &= \sqrt{2} H_d^- H_d^0 T^+ - (H_d^0)^2 T^0 - (H_d^-)^2 T^{++}, \\ H_u \cdot \bar{T} H_u &= \sqrt{2} H_u^+ H_u^0 \bar{T}^- - (H_u^0)^2 \bar{T}^0 - (H_u^+)^2 \bar{T}^{--}. \end{aligned} \quad (8)$$

III. EDMS IN THE TNMSSM

In this section, we present the EDMs of b, c quark d_b , d_c , neutron d_n , mercury d_{Hg} and electron d_e .

A. The EDMs of b, c quark d_b , d_c

The quark EDMs at the low scale Λ_χ , can be obtained from $d_q^\gamma(\Lambda_\chi)$, $d_q^g(\Lambda_\chi)$ and $C_5(\Lambda_\chi)$ by

$$d_q = d_q^\gamma(\Lambda_\chi) + \frac{e}{4\pi} d_q^g(\Lambda_\chi) + \frac{e\Lambda_\chi}{4\pi} C_5(\Lambda_\chi), \quad (9)$$

where $\Lambda_\chi = m_q$ denotes the chirality breaking scale, m_q denotes the corresponding quark mass. Weinberg discovered the supersymmetric contribution of the purely gluonic CP-violating operator to the neutron EDM, the Wilson coefficient C_5 reads [50]

$$C_5(\Lambda) = -\frac{3g_3^5}{(4\pi)^4 M_3^3} \left\{ m_t \Im[e^{2i\theta_3} (Z_{\tilde{t}})_{2,2} (Z_{\tilde{t}})^\dagger_{2,1}] \frac{x_{\tilde{t}_1} - x_{\tilde{t}_2}}{x_{M_3}} H\left(\frac{x_{\tilde{t}_1}}{x_{M_3}}, \frac{x_{\tilde{t}_2}}{x_{M_3}}, \frac{x_t}{x_{M_3}}\right) \right. \\ \left. + m_b \Im[e^{2i\theta_3} (Z_{\tilde{b}})_{2,2} (Z_{\tilde{b}})^\dagger_{2,1}] \frac{x_{\tilde{b}_1} - x_{\tilde{b}_2}}{x_{M_3}} H\left(\frac{x_{\tilde{b}_1}}{x_{M_3}}, \frac{x_{\tilde{b}_2}}{x_{M_3}}, \frac{x_b}{x_{M_3}}\right) \right\}. \quad (10)$$

Here, the $\Im[x, y]$ refers to the imaginary part of $[x, y]$, the H function can be found in Refs. [50, 51]. $Z_{\tilde{t}}$ and $Z_{\tilde{b}}$ are respectively the matrix to diagonalize the mass squared matrix of stop and sbottom. At the same time, the evolution of d_q^γ , d_q^g and C_5 with the renormalization group equations from the matching scale Λ to the chiral symmetry breaking scale Λ_χ is represented by

$$d_q^\gamma(\Lambda_\chi) = \eta^{ED} d_q^\gamma(\Lambda), \quad d_q^g(\Lambda_\chi) = \eta^{CD} d_q^g(\Lambda), \quad C_5(\Lambda_\chi) = \eta^G C_5(\Lambda). \quad (11)$$

where η^{ED} , η^{CD} , η^G represent the evolution coefficient of d_q^γ , d_q^g and C_5 with the renormalization group equations from the higher scale Λ to the low scale Λ_χ .

The effective Lagrangian for the EDM d_q of the fermion is defined through the dimension five operator [52].

$$\mathcal{L}_{EDM} = -\frac{i}{2} d_q^\gamma \bar{q} \sigma^{\mu\nu} \gamma_5 q F_{\mu\nu}, \quad (12)$$

with $\sigma^{\mu\nu} = i[\gamma^\mu, \gamma^\nu]/2$, $F_{\mu\nu}$ representing the electromagnetic field strength, q denoting a fermion field. Besides the operator in Eq. (12), the CEDM of quarks can also contribute to d_q

$$\mathcal{L}_{CEDM} = -\frac{i}{2}d_q^q \bar{q}\sigma^{\mu\nu}\gamma_5 q G_{\mu\nu}^a T^a, \quad (13)$$

where $G_{\mu\nu}$ is the $SU(3)$ gauge field strength, T^a is the $SU(3)$ generators.

We use the effective method to obtain the effective Lagrangian with the CPV operators at matching scale Λ which should be evolved down to the quark mass scale using the renormalization group equations (RGEs). The effective Lagrangian with these CPV operators relevant to the quark EDM and CEDM can be represented by Eq. (14)

$$\mathcal{L}_{eff} = \sum_i^5 C_i(\Lambda)\mathcal{O}_i(\Lambda), \quad (14)$$

with

$$\begin{aligned} \mathcal{O}_1 &= \bar{q}\sigma^{\mu\nu}P_L q F_{\mu\nu}, & \mathcal{O}_2 &= \bar{q}\sigma^{\mu\nu}P_R q F_{\mu\nu}, & \mathcal{O}_3 &= \bar{q}T^a\sigma^{\mu\nu}P_L q G_{\mu\nu}^a, \\ \mathcal{O}_4 &= \bar{q}T^a\sigma^{\mu\nu}P_R q G_{\mu\nu}^a, & \mathcal{O}_5 &= -\frac{1}{6}f_{abc}G_{\mu\rho}^a G_{\nu}^{b\rho} G_{\lambda\sigma}^c \epsilon^{\mu\nu\lambda\sigma}. \end{aligned} \quad (15)$$

$C_i(\Lambda)$ are the Wilson coefficients, like C_5 . The effective Lagrangian of quarks and squarks with gluino, neutralino and chargino are mentioned in Appendix C [53, 54].

The purely gluonic Weinberg operator O_5 originates from the two-loop "gluino-squark" diagrams. The results obtained at the matching scale Λ should be transformed down to the chirality breaking scale Λ_χ . After calculation, the following relations for the coefficients are obtained [55]

$$\begin{aligned} C_5(\Lambda_\chi) &= \mathcal{K}^{\gamma_{GG}/\beta} C_5(\Lambda), & C_\gamma(\Lambda_\chi) &= \mathcal{K}^{\gamma_q/\beta} C_\gamma(\Lambda), \\ C_q(\Lambda_\chi) &= \mathcal{K}^{\gamma_{qq}/\beta} C_q(\Lambda) + C_5(\Lambda) \frac{\gamma_{Gq} m_q(\Lambda)}{\gamma_{qq} + \gamma_m - \gamma_{GG}} (\mathcal{K}^{\gamma_{qq}/\beta} - \mathcal{K}^{(\gamma_{qq}-\gamma_m)/\beta}), \end{aligned} \quad (16)$$

with [55]

$$\begin{aligned} \mathcal{K} &= \frac{g_s(\mu)}{g_s(M)}, & \gamma(\mathcal{O}_q) &= \gamma_{qq} = \frac{29 - 2N_f}{3}, & \gamma_q &= \frac{8}{3}, \\ \gamma_{GG} &= -3 - 2N_f, & \gamma_{Gq} &= 6, & \gamma_m &= -8, & \beta &= \frac{33 - 2N_f}{3}, \end{aligned} \quad (17)$$

where N_f is the number of light quarks at scale Λ_χ . From this, the term in Eq. (9) can be further calculated using the following $C_\gamma(\Lambda)$, $C_q(\Lambda)$ and $C_5(\Lambda)$ [56]

$$\begin{aligned} d_q^\gamma &= C_\gamma(\Lambda_\chi) = \eta^{ED} C_\gamma(\Lambda), & d_q^g &= C_q(\Lambda_\chi) = \eta^{CD} C_q(\Lambda), \\ C_5(\Lambda_\chi) &= \eta^G C_5(\Lambda). \end{aligned} \quad (18)$$

Thus, it is possible to calculate the evolution coefficient in Eq.(11)

$$d_q^\gamma(\Lambda_\chi) = 1/1.53 d_q^\gamma(\Lambda), \quad d_q^g(\Lambda_\chi) = 3.3 d_q^g(\Lambda), \quad C_5(\Lambda_\chi) = 3.3 C_5(\Lambda). \quad (19)$$

The EDMs of quark can be written as

$$d_q^\gamma = -\frac{2eQ_q m_q}{(4\pi)^2} \Im(C_2^R + C_2^{L*} + C_6^R), \quad (20)$$

where $C_{2,6}^{L,R}$ represent the Wilson coefficients of the corresponding operators $O_{2,6}^{L,R}$, it is expressed as follows:

$$\begin{aligned} O_2^{L,R} &= \frac{eQ_q}{(4\pi)^2} (-iD_\alpha^*) \bar{q} \gamma^\alpha F \cdot \sigma P_{L,R} q, \\ O_6^{L,R} &= \frac{eQ_q m_q}{(4\pi)^2} \bar{q} F \cdot \sigma P_{L,R} q. \end{aligned} \quad (21)$$

Similarly, the quark CEDMs can be written as

$$d_q^g = -\frac{2g_3 m_q}{(4\pi)^2} \Im(C_7^R + C_7^{L*} + C_8^R), \quad (22)$$

where $C_{7,8}^{L,R}$ represent the Wilson coefficients of the corresponding operators $O_{7,8}^{L,R}$

$$\begin{aligned} O_7^{L,R} &= \frac{g_3}{(4\pi)^2} (-iD_\alpha^*) \bar{q} \gamma^\alpha G^a \cdot \sigma T^a P_{L,R} q, \\ O_8^{L,R} &= \frac{g_3 m_q}{(4\pi)^2} \bar{q} G^a \cdot \sigma T^a P_{L,R} q. \end{aligned} \quad (23)$$

The one-loop Feynman diagrams contributing to the above amplitudes are depicted in Fig. 1. Calculating the Feynman diagrams, d_q^γ and d_q^g at the one-loop level can be written

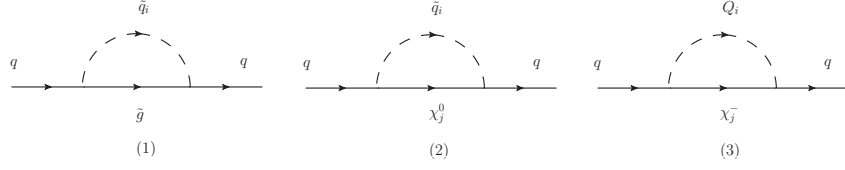


FIG. 1: The one-loop diagrams which contributes to $d_q^{\tilde{\gamma}}$ and d_q^g are obtained by attaching a photon and a gluon respectively to the internal particles in all possible ways.

as

$$\begin{aligned}
d_q^{\tilde{\gamma}(1)} &= \frac{e_q e}{12\pi^2 m_W} \frac{\sqrt{x_{\tilde{g}}}}{x_{\tilde{q}_i}} \Im \left[C_{\tilde{g}\tilde{q}_i q}^L C_{\tilde{q}_i\tilde{g}}^L \right] I_1 \left(\frac{x_{\tilde{g}}}{x_{\tilde{q}_i}} \right), \\
d_q^{g(1)} &= \frac{-g_3}{32\pi^2 m_W} \frac{\sqrt{x_{\tilde{g}}}}{x_{\tilde{q}_i}} \Im \left[C_{\tilde{g}\tilde{q}_i q}^L C_{\tilde{q}_i\tilde{g}}^L \right] I_2 \left(\frac{x_{\tilde{g}}}{x_{\tilde{q}_i}} \right), \\
d_q^{\tilde{\gamma}(2)} &= \frac{e_q e}{32\pi^2 m_W} \frac{\sqrt{x_{\chi_j^0}}}{x_{\tilde{q}_i}} \Im \left[C_{\tilde{q}_i\chi_j^0}^L C_{\tilde{\chi}_j^0\tilde{q}_i q}^R \right] I_1 \left(\frac{x_{\chi_j^0}}{x_{\tilde{q}_i}} \right), \\
d_q^{g(2)} &= \frac{g_3^3}{128\pi^2 e^2 m_W} \frac{\sqrt{x_{\chi_j^0}}}{x_{\tilde{q}_i}} \Im \left[C_{\tilde{q}_i\chi_j^0}^L C_{\tilde{\chi}_j^0\tilde{q}_i q}^R \right] I_1 \left(\frac{x_{\chi_j^0}}{x_{\tilde{q}_i}} \right), \\
d_q^{\tilde{\gamma}(3)} &= \frac{e}{16\pi^2 m_W} \frac{\sqrt{x_{\chi_j^-}}}{x_{\tilde{Q}_i}} \Im \left[C_{\tilde{q}\tilde{Q}_i\chi_j^-}^L C_{\tilde{\chi}_j^-\tilde{Q}_i q}^R \right] \left[e_Q I_1 \left(\frac{x_{\chi_j^-}}{x_{\tilde{Q}_i}} \right) + (e_q - e_Q) I_3 \left(\frac{x_{\chi_j^-}}{x_{\tilde{q}_i}} \right) \right], \\
d_q^{g(3)} &= \frac{g_3^3}{16\pi^2 e^2 m_W} \frac{\sqrt{x_{\chi_j^-}}}{x_{\tilde{Q}_i}} \Im \left[C_{\tilde{q}\tilde{Q}_i\chi_j^-}^L C_{\tilde{\chi}_j^-\tilde{Q}_i q}^R \right] I_1 \left(\frac{x_{\chi_j^-}}{x_{\tilde{Q}_i}} \right), \tag{24}
\end{aligned}$$

where x_i denotes m_i^2/m_W^2 , g_3 is the strong coupling constant, $C_{abc}^{L,R}$ denotes the constant parts of the interaction vertex about abc which can be obtained through SARAH [57–61], and a, b, c denote the interacting particles. We will provide the functions $I_{1,2,3}$ in Appendix B.

The two-loop gluino corrections to the Wilson coefficients from the self-energy diagrams for quarks are considered, the corresponding Feynman diagrams are depicted in Fig. 2. The corresponding dipole moment diagrams are obtained by attaching a photon or gluon to the internal particles in all possible ways. Then the contributions from these two-loop diagrams

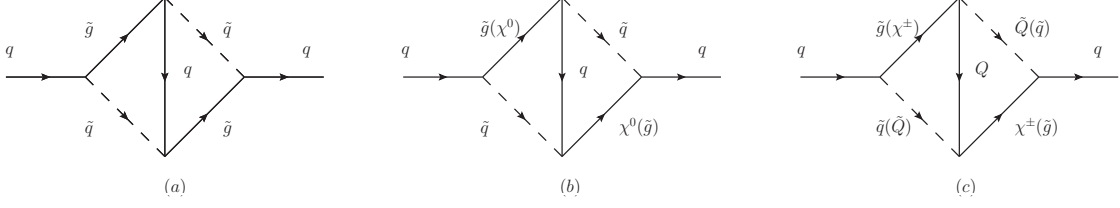


FIG. 2: The two-loop diagrams which contributes to d_q^γ and d_q^g are obtained by attaching a photon and a gluon respectively to the internal particles in all possible ways.

to d_q^γ and d_q^g can be written as

$$\begin{aligned}
d_q^{\gamma(a)} &= \frac{-4e_q e g_3^2 |m_{\tilde{g}}|}{9(4\pi)^4 m_W^2} F_3(x_q, x_{\tilde{q}_j}, x_{\tilde{g}}, x_{\tilde{g}}, x_{\tilde{q}_i}) \Im[C_{\tilde{q}\tilde{g}\tilde{q}_j}^L C_{\tilde{g}\tilde{q}\tilde{q}_j}^L], \\
d_q^{g(a)} &= d_q^{\gamma(a)} g_3 / (e_q e), \\
d_q^{\gamma(b)} &= \frac{4e_q e}{3(4\pi)^4 m_W^2} \left\{ |m_{\tilde{g}}| F_4(x_q, x_{\tilde{q}_j}, x_{\tilde{g}}, x_{\chi_k^0}, x_{\tilde{q}_i}) \Im[C_{\tilde{\chi}_k^0 q \tilde{q}_j}^R C_{\tilde{\chi}_k^0 q \tilde{q}_i}^L C_{\tilde{g}\tilde{q}\tilde{q}_j}^L C_{\tilde{g}\tilde{q}\tilde{q}_i}^L - C_{\tilde{\chi}_k^0 q \tilde{q}_j}^L \right. \\
&\quad \times C_{\tilde{\chi}_k^0 q \tilde{q}_i}^R C_{\tilde{q}\tilde{g}\tilde{q}_j}^{L*} C_{\tilde{q}\tilde{g}\tilde{q}_i}^{L*}] - m_{\chi_k^0} F_5(x_q, x_{\tilde{q}_j}, x_{\tilde{g}}, x_{\chi_k^0}, x_{\tilde{q}_i}) \Im[C_{\tilde{\chi}_k^0 q \tilde{q}_j}^R C_{\tilde{\chi}_k^0 q \tilde{q}_i}^R C_{\tilde{q}\tilde{g}\tilde{q}_j}^{L*} C_{\tilde{q}\tilde{g}\tilde{q}_i}^L \\
&\quad \left. - C_{\tilde{\chi}_k^0 q \tilde{q}_j}^L C_{\tilde{\chi}_k^0 q \tilde{q}_i}^L C_{\tilde{q}\tilde{g}\tilde{q}_i}^{L*} C_{\tilde{g}\tilde{q}\tilde{q}_j}^L] \right\}, \\
d_q^{g(b)} &= d_q^{\gamma(b)} g_3 / (e_q e), \\
d_q^{\gamma(c)} &= \frac{2e}{3(4\pi)^4 m_W^2} \left\{ |m_{\tilde{g}}| F_4(x_Q, x_{\tilde{Q}_j}, x_{\tilde{g}}, x_{\chi_k^\pm}, x_{\tilde{q}_i}) \Im[C_{\tilde{Q}\tilde{\chi}_k^\pm \tilde{q}_j}^L C_{\tilde{Q}\tilde{\chi}_k^\pm \tilde{q}_i}^R C_{\tilde{g}\tilde{Q}\tilde{Q}_j}^L C_{\tilde{g}\tilde{Q}\tilde{Q}_i}^L - C_{\tilde{Q}\tilde{\chi}_k^\pm \tilde{q}_j}^R \right. \\
&\quad \times C_{\tilde{Q}\tilde{\chi}_k^\pm \tilde{q}_i}^L C_{\tilde{Q}\tilde{g}\tilde{Q}_j}^{L*} C_{\tilde{Q}\tilde{g}\tilde{Q}_i}^{L*}] - m_{\chi_k^\pm} F_5(x_Q, x_{\tilde{Q}_j}, x_{\tilde{g}}, x_{\chi_k^\pm}, x_{\tilde{q}_i}) \Im[C_{\tilde{Q}\tilde{\chi}_k^\pm \tilde{q}_j}^L C_{\tilde{Q}\tilde{\chi}_k^\pm \tilde{q}_i}^L C_{\tilde{Q}\tilde{g}\tilde{Q}_j}^{L*} C_{\tilde{g}\tilde{Q}\tilde{Q}_i}^L \\
&\quad \left. - C_{\tilde{Q}\tilde{\chi}_k^\pm \tilde{q}_j}^R C_{\tilde{Q}\tilde{\chi}_k^\pm \tilde{q}_i}^R C_{\tilde{g}\tilde{Q}\tilde{Q}_i}^L C_{\tilde{q}\tilde{g}\tilde{Q}_j}^{L*}] \right\}, \\
d_q^{g(c)} &= d_q^{\gamma(c)} g_3 / e, \tag{25}
\end{aligned}$$

where the concrete expressions for the functions $F_{3,4,5}$ can be found in Ref. [62].

We should note that there are infrared divergencies in Fig. 2 when the SM quarks appear as internal particles, because we calculate these diagrams by expanding the external momentum. In this case, matching full theory diagrams to the corresponding two-loop diagrams in Fig. 2 is needed to cancel the infrared divergency. Taking Fig. 2(a) as example to illustrate how to cancel the infrared divergency, the corresponding diagrams are shown in Fig. 3. When the external gluon is attached to an internal particle in Fig. 2(a), and the external gluon can be attached to the same internal particle in Fig. 3(a) or (b). Then infrared divergency in the diagram by attaching a gluon in Fig. 2(a) can be cancelled by

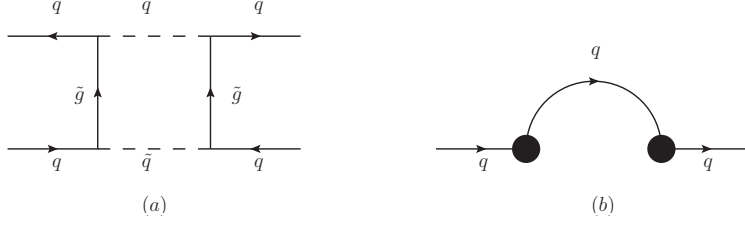


FIG. 3: Full theory diagram (a) and effective diagram (b) are plotted, where the blobs denote the effective vertexes, and an outgoing photon or gluon is attached by all possible ways.

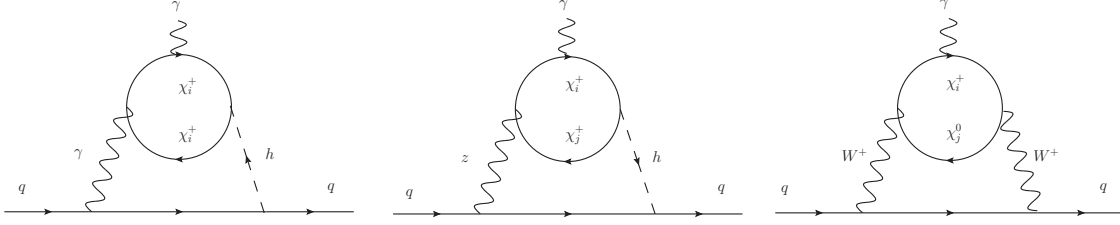


FIG. 4: The two-loop Barr-Zee type diagrams contributing to the quark EDM. The diagrams in which the photon or gluon is emitted from the W boson or the internal fermion do not contribute to the quark EDM or CEDM.

subtracting the corresponding diagram by attaching a gluon in the same way in Fig. 3.

In addition, the two-loop Barr-Zee type diagrams can also make contributions to the quark EDM. The diagrams in which a closed fermion loop is attached to the virtual gauge bosons or Higgs fields are considered, and the corresponding Feynman diagrams are depicted in Fig. 4. Then, the contributions from these two-loop Barr-Zee type diagrams to d_q^γ are given by [63]

$$\begin{aligned}
d_q^{\gamma h} &= \frac{e_q e^3}{32\pi^4 m_W} \frac{\sqrt{x_{\chi_i^+}}}{x_{h_k}} \Im \left[C_{\bar{\chi}_i^+ h \chi_i^+}^R C_{\bar{q} h_k q} \right] f_{\gamma H} \left(\frac{x_{\chi_i^+}}{x_{h_k}} \right), \\
d_q^{z h} &= \frac{e^2 (T_{3q} - 2e_q s_w^2)}{128\pi^4 c_w s_w m_W} \frac{\sqrt{x_{\chi_i^+}}}{x_{h_k}} \Im \left[\left(C_{\bar{\chi}_j^+ h_k \chi_i^+}^R C_{\bar{\chi}_i^+ Z \chi_j^+}^L - C_{\bar{\chi}_j^+ h_k \chi_i^+}^L C_{\bar{\chi}_i^+ Z \chi_j^+}^R \right) C_{\bar{q} h_k q} \right] \\
&\quad * f_{ZH} \left(\frac{x_Z}{x_{h_k}}, \frac{x_{\chi_i^+}}{x_{h_k}}, \frac{x_{\chi_j^+}}{x_{h_k}} \right), \\
d_q^{WW} &= \frac{T_{3q} e^3}{128\pi^4 s_w^2 m_W} \sqrt{x_q x_{\chi_i^+} x_{\chi_j^0}} \Im \left[C_{\bar{\chi}_j^0 W_\mu^+ \chi_i^+}^R C_{\bar{\chi}_j^0 W_\mu^+ \chi_i^+}^{L*} \right] f_{WW} \left(x_{\chi_i^+}, x_{\chi_j^0} \right), \quad (26)
\end{aligned}$$

where $s_w \equiv \sin \theta_W$, $c_w \equiv \cos \theta_W$, and θ_W is the Weinberg angle, T_{3q} denotes the isospin of

the corresponding quark, the functions $f_{\gamma H}$, f_{ZH} , f_{WW} can be found in Ref. [63].

B. The EDM of neutron d_n and mercury d_{Hg}

To be consistent with the discussion in Ref. [22], for the neutron EDM d_n , we adopt the values 0.5 and 12 MeV for the coefficients 1 ± 0.5 and 22 ± 10 MeV in Eq. (2) respectively. C_5 in Eq. (2) can be obtained in Eq.(11) and Eq.(19). d_q^g and d_q^γ in Eq. (2) have three contributions: from one-loop Feynman diagrams contributions in Fig. 1, which can be obtained in Eq.(24), from two-loop Feynman diagrams contributions in Fig. 2, which can be obtained in Eq.(25) and from two-loop Barr-Zee type diagrams contributions in Fig. 4, which can be obtained in Eq.(26).

According to the Ref. [65], where it was shown that the dominant contribution arises from the CEDMs of quarks (d_q^g) according to

$$d_{Hg} = - (d_d^g - d_u^g - 0.012d_s^g) \times 3.2 \cdot 10^{-2} e . \quad (27)$$

d_q^g can be obtained in Eq.(11), Eq.(24) and Eq.(26), where $x_i = m_i^2/m_W^2$, $C_{abc}^{L,R}$ denotes the constant parts of the interaction vertex about abc which can be obtained through SARAH [57–61], and a, b, c denote the interacting particles. We will provide the functions $I_{1,2,3}$ in Appendix B.

C. The EDM of electron d_e

The effective Lagrangian for the electron EDM can be written as

$$\mathcal{L}_{EDM} = -\frac{i}{2} d_e \bar{l}_e \sigma^{\mu\nu} \gamma_5 l_e F_{\mu\nu}, \quad (28)$$

where $\sigma^{\mu\nu} = i[\gamma^\mu, \gamma^\nu]/2$, $F_{\mu\nu}$ is the electromagnetic field strength, and l_e denotes the electron which is on-shell. The electron EDMs can be written as

$$d_e = -\frac{2eQ_f m_e}{(4\pi)^2} \Im(C_2^R + C_2^{L*} + C_6^R), \quad (29)$$

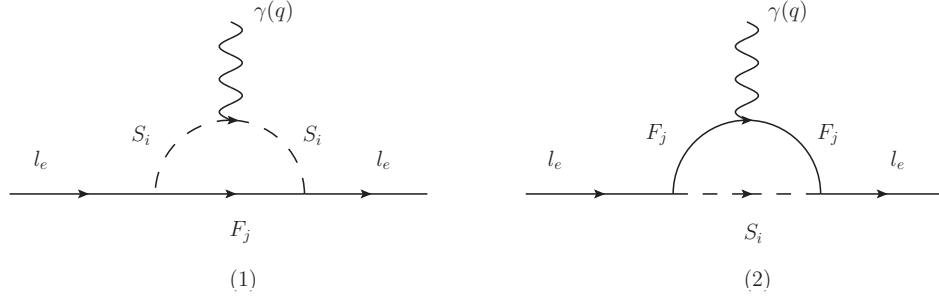


FIG. 5: The one-loop Feynman diagrams contributing to the electron EDM, where (1) denotes a charged scalar loop, and (2) denotes a charged fermion loop.

where $C_{2,6}^{L,R}$ represent the Wilson coefficients of the corresponding operators $O_{2,6}^{L,R}$, it is expressed as follows:

$$\begin{aligned}
O_2^{L,R} &= \frac{eQ_q}{(4\pi)^2} (-iD_\alpha^*) \bar{l}_e \gamma^\mu F \cdot \sigma P_{L,R} l_e, \\
O_6^{L,R} &= \frac{eQ_q m_e}{(4\pi)^2} \bar{l}_e F \cdot \sigma P_{L,R} l_e,
\end{aligned} \tag{30}$$

The one-loop Feynman diagrams contributing to the electron EDM are depicted in Fig. 5. Calculating the Feynman diagrams, d_e at the one-loop level can be written as

$$\begin{aligned}
d_e^{(1)} &= \frac{-2}{em_e} \Im \left\{ x_e [-I_3(x_{F_j}, x_{S_i}) + I_4(x_{F_j}, x_{S_i})] [(C_{\bar{l}_e S_i F_j}^L C_{\bar{F}_j S_i l_e}^R) + (C_{\bar{l}_e S_i F_j}^R C_{\bar{F}_j S_i l_e}^L)^*] \right. \\
&\quad \left. + \sqrt{x_e x_{F_j}} [-2I_1(x_{F_j}, x_{S_i}) + 2I_3(x_{F_j}, x_{S_i})] C_{\bar{l}_e S_i F_j}^R C_{\bar{F}_j S_i l_e}^R \right\}, \\
d_e^{(2)} &= \frac{-2}{em_e} \Im \left\{ x_e [-I_1(x_{F_j}, x_{S_i}) + 2I_3(x_{F_j}, x_{S_i}) - I_4(x_{F_j}, x_{S_i})] [(C_{\bar{l}_e S_i F_j}^R C_{\bar{F}_j S_i l_e}^L) \right. \\
&\quad \left. + (C_{\bar{l}_e S_i F_j}^L C_{\bar{F}_j S_i l_e}^R)^*] + \sqrt{x_e x_{F_j}} [2I_1(x_{F_j}, x_{S_i}) - 2I_2(x_{F_j}, x_{S_i}) - 2I_3(x_{F_j}, x_{S_i})] \right. \\
&\quad \left. \times C_{\bar{l}_e S_i F_j}^R C_{\bar{F}_j S_i l_e}^R \right\}, \\
d_e &= d_e^{(1)} + d_e^{(2)},
\end{aligned} \tag{31}$$

where $x_i = m_i^2/m_W^2$, $C_{abc}^{L,R}$ denotes the constant parts of the interactional vertex about abc , which can be got through SARAH, the interacting particles are denoted by a, b, c . And the specific expressions for the functions $I_{1,2,3,4}$ is given by Refs. [66, 67]. For completeness, we will provide the specific forms of $C_{abc}^{L,R}$ and $I_{1,2,3,4}$ in Appendix B.

IV. NUMERICAL ANALYSES

In this section, we provide the numerical results of EDMs d_n , d_b , d_c , d_e and d_{Hg} in the TNMSSM. For SM parameters, we take the W boson mass $m_W = 80.337$ GeV, the Z boson mass $m_Z = 91.1876$ GeV, the u quark mass $m_u = 2.2$ MeV, the d quark mass $m_d = 4.7$ MeV, the b quark mass $m_b = 4.18$ GeV, the c quark mass $m_c = 1.27$ GeV, $\alpha_{em}(m_Z) = 1/128.9$ for the coupling of the electromagnetic interaction, $\alpha_s(m_Z) = 0.118$ for the coupling of the strong interaction [68–76]. According to the analysis in Ref. [64, 77, 78], we take $\tan \beta' = 1.3$, $v_T^2 + v_T^{\prime 2} = 1 GeV^2$. According to the analysis in Ref. [79], we take the mass of gluino larger than 2 TeV. For the squark sector, we take $m_{\tilde{q}} = m_{\tilde{u}} = m_{\tilde{d}} = \text{diag}(M_Q, M_Q, M_Q)$ TeV and $T_{u,d} = Y_{u,d} \text{diag}(A_Q, A_Q, A_Q)$ TeV for simplicity. The observed Higgs signal limits that $M_Q > 1.5$ TeV [80]. Considering the experimental constraints described in Eq. (1) and Eq. (3), we adopt the following parameters to carry out the numerical calculation

$$\begin{aligned} \tan \beta &= 5, \quad \tan \beta' = 1.3, \quad \lambda_T = -0.22, \quad \kappa = 0.8, \quad \chi_d = \chi_t = 0.1, \\ T_\lambda &= T_{\lambda_T} = -0.1 \text{ TeV}, \quad |M_1| = 0.5 \text{ TeV}, \quad |M_2| = 0.6 \text{ TeV}, \\ T_{\chi_t} &= -0.8 \text{ TeV}, \quad T_{\chi_d} = -0.5 \text{ TeV}. \end{aligned} \quad (32)$$

Then we calculate the contributions from one loop diagrams and the Weinberg operators of neutron (d_n), b quark (d_b), c quark (d_c), electron (d_e) and mercury (d_{Hg}). To explore the effects of θ_3 (the phase angle of gluino mass M_3) and μ term makes the dominant contributions to the EWB [15], and the corresponding CPV phase θ_μ is requested to be large. We plot d_n versus θ_3 in Fig. 6 (a) and θ_μ in Fig. 6 (b), where the shaded area represent the experimental range of d_n , the black solid, black dashed, black dotted lines in in Fig. 6 (a) denotes the results for $M_3 = 4.00, 4.25, 4.50$ TeV respectively, the black solid, black dashed, black dotted lines in in Fig. 6 (b) denotes the results for $\mu = 1.2, 1, 0.8$ TeV respectively. Similarly, we plot d_b versus θ_3 in Fig. 6 (c), d_b versus θ_μ in Fig. 6 (d), d_c versus θ_3 in Fig. 6 (e), d_c versus θ_μ in Fig. 6 (f), d_e versus θ_3 in Fig. 6 (g), d_e versus θ_μ in Fig. 6 (h), d_{Hg} versus θ_3 in Fig. 6 (i), d_{Hg} versus θ_μ in Fig. 6 (j). The red lines in Fig. 6 denote the results predicted in the MSSM with the same parameter space.

From the picture, it is obvious that the results for $d_n, d_b, d_c, d_e, d_{Hg}$ predicted in the TN-

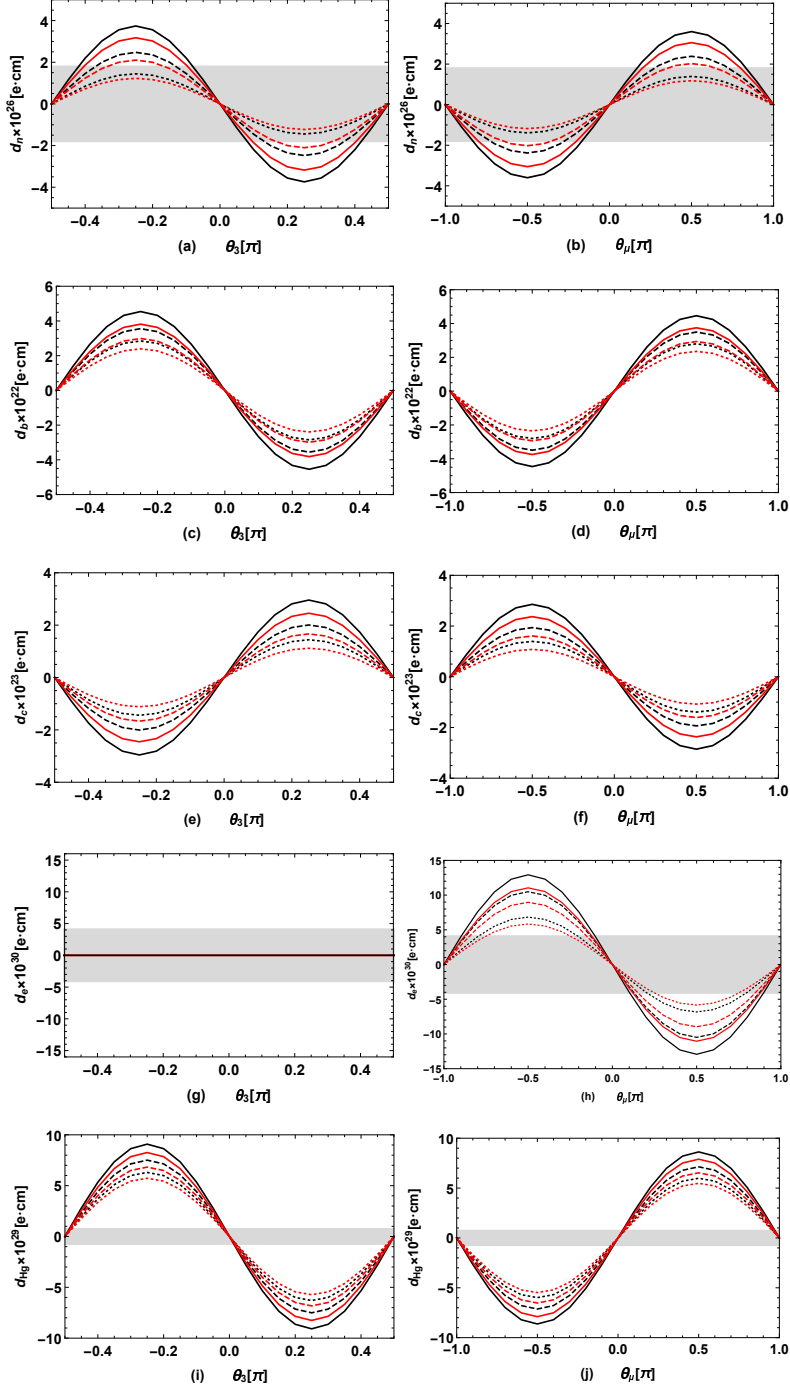


FIG. 6: Take the values from Eq. (32), d_n , d_b , d_c , d_e , d_{Hg} versus θ_3 , θ_μ are plotted, where the solid, dashed and dotted lines denote the results for $M_3 = 4.00, 4.25, 4.50$ TeV respectively for (a), (c), (e), (g), (i) and the results for $\mu = 1.2, 1, 0.8$ TeV respectively for (b), (d), (f), (h), (j). Similarly, the results predicted in the MSSM with the same parameter space are denoted by the red lines.

MSSM are larger than the ones predicted in the MSSM, because the additional neutralinos, charginos, the redefinitions of squark mass matrices and the μ term can make contributions to these EDMs. In addition, the effects of θ_3, θ_μ on $d_n, d_b, d_c, d_e, d_{Hg}$ can be amplified for larger M_3 and larger μ respectively, it indicates these EDMs increase with increasing M_3, μ for fixed θ_3 and θ_μ , the fact can be seen explicitly in Fig. 6. Due to the strict upper bound on d_n experimentally, θ_3, θ_μ are limited to be very small for large M_3 and μ respectively, while they are not constrained by the upper bounds on d_b, d_c, d_e, d_{Hg} in the same parameter space as shown in Fig. 6 (c), (d), (e), (f), (g), (h), (i), (j).

Comparing with the MSSM, there are two new CPV sources χ_d and χ_t in the TNMSSM, which can also make contributions to the considered EDMs $d_n, d_b, d_c, d_e, d_{Hg}$. To see explicitly their effects on $d_n, d_b, d_c, d_e, d_{Hg}$, we assume all contributions to these EDMs come from θ_d, θ_t and scan the the following parameter space

$$\chi_d = (-1, 1), \chi_t = (-1, 1), \theta_d = (-\pi, \pi), \theta_t = (-\pi, \pi). \quad (33)$$

Taking the parameters in Eq. (32) as inputs, we plot d_n versus χ_t, θ_t in Fig. 7 (a), (b) respectively, where the shaded area represent the experimental range of d_n , the red lines denote the results predicted in the MSSM with the same parameter space (which is 0 in this case because there is no such CPV sources in the MSSM). Similarly, we plot d_b, d_c, d_e and d_{Hg} versus χ_t, θ_t in Fig. 7 (c, d), (e, f), (g, h), (i, j) respectively. There are no shaded area in Fig. 7 (c, d), (e, f), (g, h), (i, j) because the upper bounds on d_b, d_c, d_e and d_{Hg} are much larger than the results shown in the picture.

From Eq. (A1) to Eq. (A6), it can be noted that the effects of χ_t are enhanced by $\tan \beta$ compared to the ones of χ_d , and dominant contributions to these EDMs come from the up-type squarks which related directly to χ_t . As a result, χ_t affects the numerical results of $d_n, d_b, d_c, d_e, d_{Hg}$ much more acutely than the ones of χ_d , the fact can be seen explicitly in Fig. 7 because the predicted $d_n, d_b, d_c, d_e, d_{Hg}$ approach to 0 when $\theta_t = 0$. Fig. 7 (a, b) show that the new CPV source χ_t also suffer the constraints from the experimental upper bound on d_n , and the constraints on θ_t can be relaxed when $|\chi_t| \lesssim 0.2$. In addition, the theoretical predictions on d_b, d_c can reach 10^{-26} e-cm, 10^{-27} e-cm, d_e, d_{Hg} can reach 10^{-31} e-cm, 10^{-29} e-cm respectively when the contributions come from the new CPV effects in the

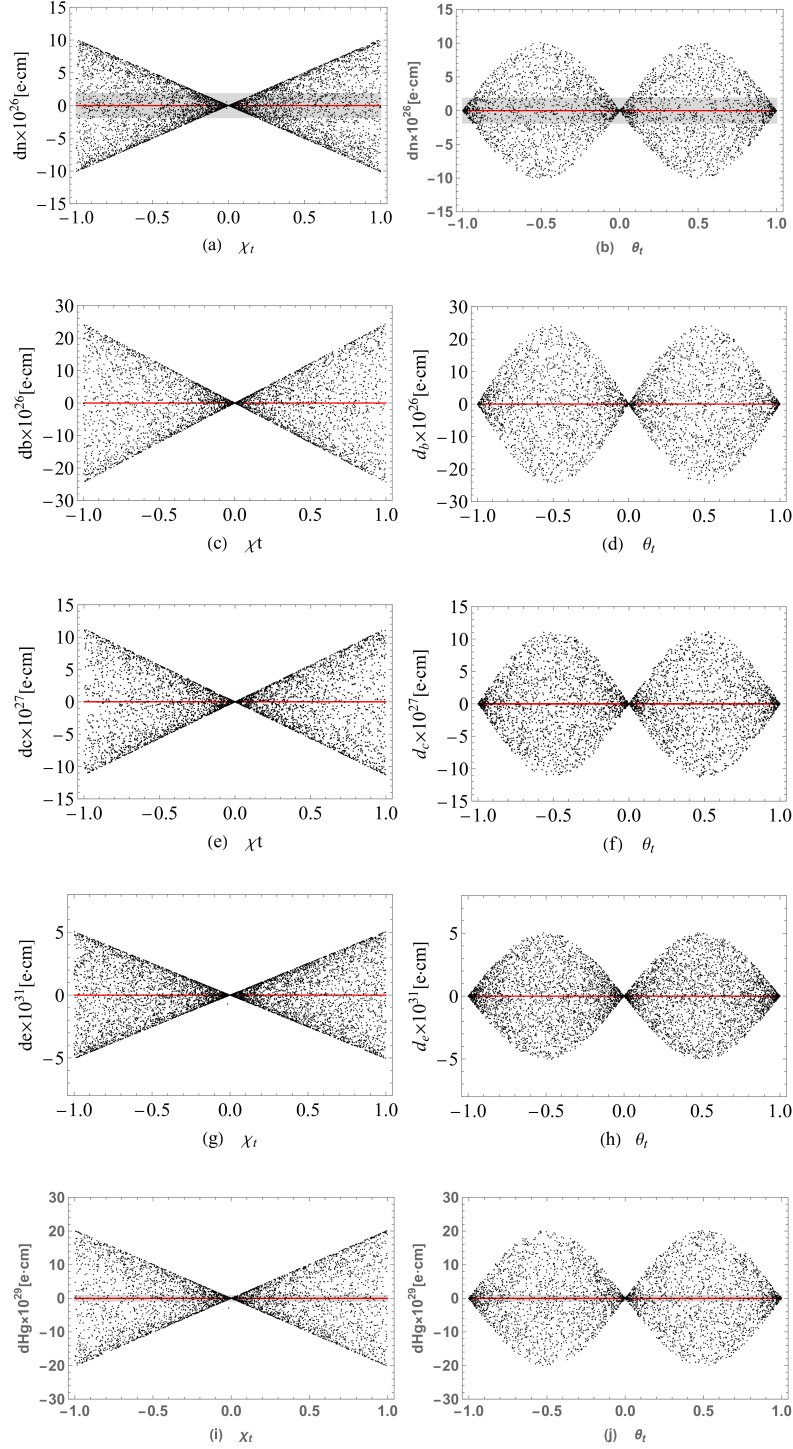


FIG. 7: Scanning the parameter space shown in Eq. (33), d_n , d_b , d_c , d_e and d_{Hg} versus χ_t , θ_t are plotted, where the red lines denote the corresponding MSSM predictions in the same parameter space and the shaded areas represent the experimental upper bound on d_n .

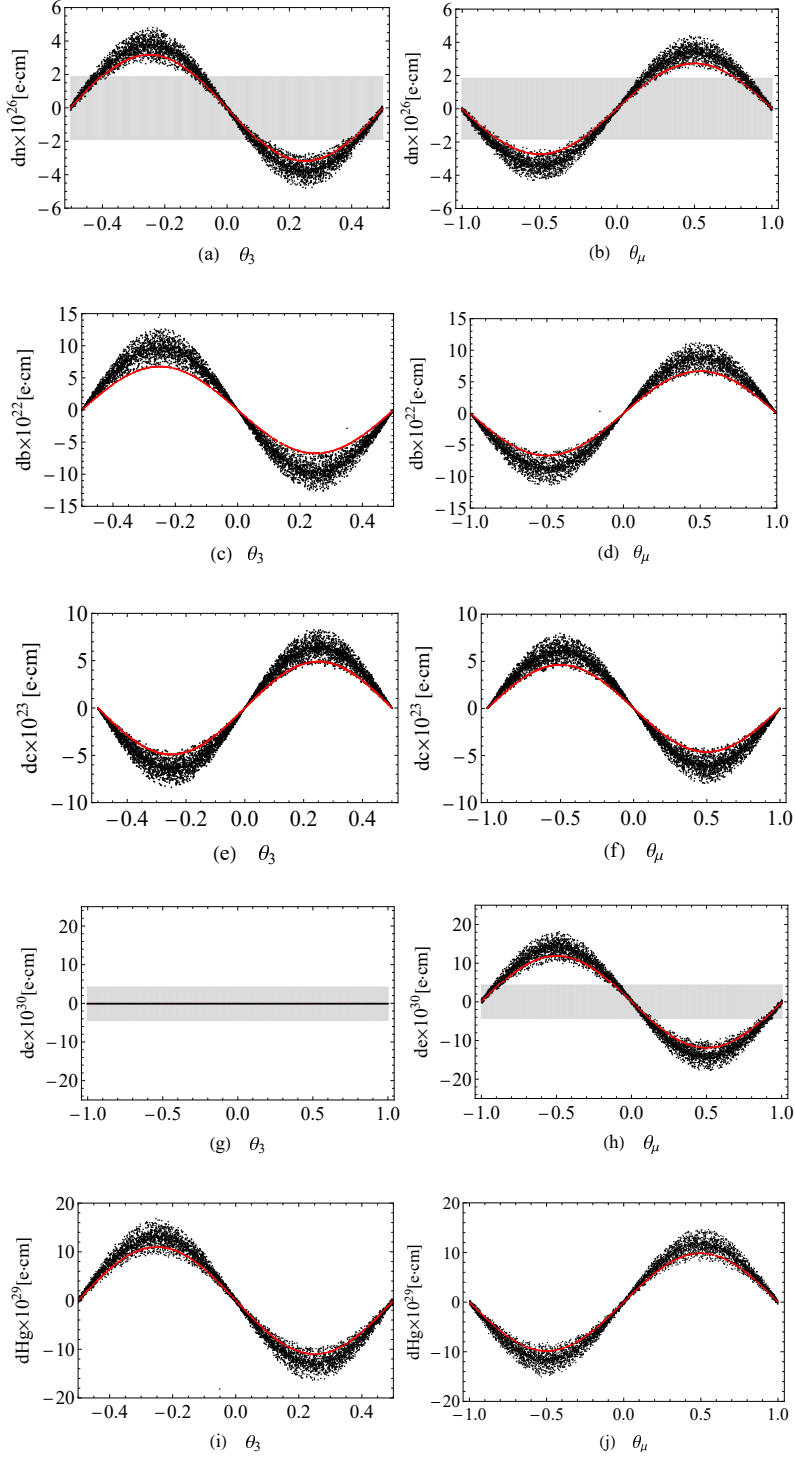


FIG. 8: Scanning the parameter space shown in Eq. (33), d_n , d_b , d_c , d_e and d_{Hg} versus θ_3 , θ_μ are plotted, where the red lines denote the corresponding MSSM predictions in the same parameter space and the shaded areas represent the experimental range of d_n and d_e

TNMSSM, which has the potential to be verified experimentally in future.

To see the combining effects of the new CPV sources χ_d, χ_t in the TNMSSM and the traditional CPV sources M_3, μ in SUSY models on $d_n, d_b, d_c, d_e, d_{Hg}$, we set $M_3 = 5$ TeV, $\mu = 0.6$ and scan the parameter space in Eq. (33). Taking $\theta_\mu = 0$, we plot d_n versus θ_3 in Fig. 8 (a), where the red line denotes the corresponding MSSM prediction in the same parameter space, the shaded area represents the experimental upper bound on d_n . Similarly, d_n versus θ_μ for $\theta_3 = 0$ are plotted in Fig. 8 (b), and d_b versus θ_3, d_b versus θ_μ, d_c versus θ_3, d_c versus θ_μ, d_e versus θ_3, d_e versus θ_μ, d_{Hg} versus θ_3, d_{Hg} versus θ_μ are plotted in Fig. 8 (c), (d), (e), (f), (g), (h), (i), (j) respectively, the shaded area represents the experimental upper bound on d_e . The picture shows explicitly that the new CPV sources in the TNMSSM can make important contributions to the EDMs $d_n, d_b, d_c, d_e, d_{Hg}$, and these EDMs predicted in the TNMSSM are much larger than the ones predicted in the MSSM shown by the red lines in Fig. 8. In addition, the effects of the new CPV sources χ_d, χ_t are related closely to M_3 and μ , because they affect the numerical results slightly when θ_3 or θ_μ approaches to 0 as shown in Fig. 8. By comparing the (g, h), (i, j) with (a, b) in Fig. 6 and Fig. 8, it can be observed that the phase θ_μ of the coupling μ is quite constrained by the experimental limits on the electron EDM and mercury EDM. And d_e, d_{Hg} also have stronger restrictions on θ_μ than that on d_n .

V. SUMMARY

In this work, we study and analyze the EDMs of neutron, electron, mercury and heavy quarks b, c in the TNMSSM. The redefined μ term and squark mass matrices, the new introduced CPV sources χ_d, χ_t in the TNMSSM can make contributions to these EDMs. We calculate the loop-induced contributions through the effective theory, and all contributions are presented as the coefficients of effective operators. Considering the latest upper bounds on the EDMs $d_n, d_e, d_{Hg}, d_b, d_c$ and focusing on the TNMSSM-specialized CPV sources, we carry out the numerical analysis properly. It is found that the theoretical predictions on $d_n, d_e, d_{Hg}, d_b, d_c$ in the TNMSSM are much different from the ones in the MSSM due to the presence of new particles and new CPV sources in the TNMSSM, where the new CPV

source χ_t in the TNMSSM can make significant contributions to these EDMs. In addition, the parameter space of the TNMSSM can be limited by the experimental upper bound on d_n , d_e and d_{Hg} , the predicted d_b , d_c can reach 10^{-22} e-cm, 10^{-23} e-cm respectively which have the potential to be verified experimentally in future[64, 81, 82].

Acknowledgments

The work has been supported by the National Natural Science Foundation of China (NNSFC) with Grants No. 12075074, No. 12235008, Hebei Natural Science Foundation with Grant No. A2022201017, No. A2023201041, Natural Science Foundation of Guangxi Autonomous Region with Grant No. 2022GXNSFDA035068, the youth top-notch talent support program of the Hebei Province.

Appendix A: New definitions of some mass matrixes in the TNMSSM.

In the TNMSSM, the dominant contributions to d_n , d_b , d_c come from squarks, sgluon, neutralinos and charginos. To see the new contributions in the model to these EDMS clearly, we present the new definitions of the relevant mass matrixes. On the basis $(\tilde{d}_{L,\alpha_1}^0, \tilde{d}_{R,\alpha_2}^0)$, $(\tilde{d}_{L,\beta_1}^{0,*}, \tilde{d}_{R,\beta_2}^{0,*})$, the definition of the squared mass matrix for down type squark is given by [57]

$$M_D^2 = \begin{pmatrix} m_{\tilde{d}_L^0 \tilde{d}_L^{0,*}} & m_{\tilde{d}_R^0 \tilde{d}_L^{0,*}}^\dagger \\ m_{\tilde{d}_L^0 \tilde{d}_R^{0,*}} & m_{\tilde{d}_R^0 \tilde{d}_R^{0,*}} \end{pmatrix}, \quad (\text{A1})$$

where

$$\begin{aligned} m_{\tilde{d}_L^0 \tilde{d}_L^{0,*}} &= -\frac{1}{24} \left((3g_2^2 + g_1^2)(2v_T^2 - 2v_T^2 - v_u^2 + v_d^2) \right) + \frac{1}{2} (2m_q^2 + v_d^2 Y_d Y_d^\dagger), \\ m_{\tilde{d}_L^0 \tilde{d}_R^{0,*}} &= \frac{1}{2} \left(\sqrt{2} v_d T_d + Y_d (2v_d v_T \chi_d^* - v_s v_u \lambda^*) \right), \\ m_{\tilde{d}_R^0 \tilde{d}_R^{0,*}} &= \frac{1}{12} g_1^2 (-2v_T^2 + 2v_T^2 - v_d^2 + v_u^2) + \frac{1}{2} (2m_d^2 + v_d^2 Y_d Y_d^\dagger). \end{aligned} \quad (\text{A2})$$

On the basis $(\tilde{u}_{L,\alpha_1}^0, \tilde{u}_{R,\alpha_2}^0)$, $(\tilde{u}_{L,\beta_1}^{0,*}, \tilde{u}_{R,\beta_2}^{0,*})$, the squared mass matrix of up type squarks

is [58]

$$M_{\tilde{U}}^2 = \begin{pmatrix} m_{\tilde{u}_L^0 \tilde{u}_L^{0,*}} & m_{\tilde{u}_R^0 \tilde{u}_L^{0,*}}^\dagger \\ m_{\tilde{u}_L^0 \tilde{u}_R^{0,*}} & m_{\tilde{u}_R^0 \tilde{u}_R^{0,*}} \end{pmatrix}, \quad (\text{A3})$$

where

$$\begin{aligned} m_{\tilde{u}_L^0 \tilde{u}_L^{0,*}} &= -\frac{1}{24} \left((-3g_2^2 + g_1^2)(2v_{\tilde{T}}^2 - 2v_T^2 - v_u^2 + v_d^2) \right) + \frac{1}{2} (2m_q^2 + v_u^2 Y_u Y_u^\dagger), \\ m_{\tilde{u}_L^0 \tilde{u}_R^{0,*}} &= \frac{1}{2} \left(\sqrt{2} v_u T_u + Y_u (2v_{\tilde{T}} v_u \chi_t^* - v_d v_s \lambda^*) \right), \\ m_{\tilde{u}_R^0 \tilde{u}_R^{0,*}} &= \frac{1}{6} g_1^2 (2v_{\tilde{T}}^2 - 2v_T^2 - v_u^2 + v_d^2) + \frac{1}{2} (2m_u^2 + v_u^2 Y_u Y_u^\dagger). \end{aligned} \quad (\text{A4})$$

On the basis $(\tilde{\lambda}_B, \tilde{W}^0, \tilde{H}_d^0, \tilde{H}_u^0, \tilde{S}, \tilde{T}^0, \tilde{T}^0)$, the mass matrix for neutralinos is [59]

$$m_{\tilde{\chi}^0}^2 = \begin{pmatrix} M_1 & 0 & -\frac{1}{2} g_1 v_d & \frac{1}{2} g_1 v_u & 0 & g_1 v_T & -g_1 v_{\tilde{T}} \\ 0 & M_2 & \frac{1}{2} g_2 v_d & -\frac{1}{2} g_2 v_u & 0 & -g_2 v_T & g_2 v_{\tilde{T}} \\ -\frac{1}{2} g_1 v_d & \frac{1}{2} g_2 v_d & \sqrt{2} v_T \chi_d & -\frac{1}{\sqrt{2}} v_s \lambda & -\frac{1}{\sqrt{2}} v_u \lambda & \sqrt{2} v_d \chi_d & 0 \\ \frac{1}{2} g_1 v_u & -\frac{1}{2} g_2 v_u & -\frac{1}{\sqrt{2}} v_s \lambda & \sqrt{2} v_{\tilde{T}} \chi_t & -\frac{1}{\sqrt{2}} v_d \lambda & 0 & \sqrt{2} v_u \chi_t \\ 0 & 0 & -\frac{1}{\sqrt{2}} v_u \lambda & -\frac{1}{\sqrt{2}} v_d \lambda & \sqrt{2} v_s \kappa & -\frac{1}{\sqrt{2}} \lambda_T v_{\tilde{T}} & -\frac{1}{\sqrt{2}} \lambda_T v_T \\ g_1 v_T & -g_2 v_T & \sqrt{2} v_d \chi_d & 0 & -\frac{1}{\sqrt{2}} \lambda_T v_{\tilde{T}} & 0 & -\frac{1}{\sqrt{2}} \lambda_T v_s \\ -g_1 v_{\tilde{T}} & g_2 v_{\tilde{T}} & 0 & \sqrt{2} v_u \chi_t & -\frac{1}{\sqrt{2}} \lambda_T v_T & -\frac{1}{\sqrt{2}} \lambda_T v_s & 0 \end{pmatrix}. \quad (\text{A5})$$

On the basis $(\tilde{W}^-, \tilde{H}_d^-, \tilde{T}^-), (\tilde{W}^+, \tilde{H}_u^+, \tilde{T}^+)$, the mass matrix for charginos is [60, 61]

$$m_{\tilde{\chi}^\pm} = \begin{pmatrix} M_2 & \frac{1}{\sqrt{2}} g_2 v_u & g_2 v_T \\ \frac{1}{\sqrt{2}} g_2 v_d & \frac{1}{\sqrt{2}} v_s \lambda & -v_d \chi_d \\ g_2 v_{\tilde{T}} & -v_u \chi_t & \frac{1}{\sqrt{2}} \lambda_T v_s \end{pmatrix}. \quad (\text{A6})$$

In the basis $(\phi_d, \phi_u, \phi_s, \phi_T, \phi_{\tilde{T}})$, the definition of mass squared matrix for neutral Higgs is given by

$$m_h^2 = \begin{pmatrix} m_{\phi_d \phi_d} & m_{\phi_u \phi_d} & m_{\phi_s \phi_d} & m_{\phi_T \phi_d} & m_{\phi_{\tilde{T}} \phi_d} \\ m_{\phi_d \phi_u} & m_{\phi_u \phi_u} & m_{\phi_s \phi_u} & m_{\phi_T \phi_u} & m_{\phi_{\tilde{T}} \phi_u} \\ m_{\phi_d \phi_s} & m_{\phi_u \phi_s} & m_{\phi_s \phi_s} & m_{\phi_T \phi_s} & m_{\phi_{\tilde{T}} \phi_s} \\ m_{\phi_d \phi_T} & m_{\phi_u \phi_T} & m_{\phi_s \phi_T} & m_{\phi_T \phi_T} & m_{\phi_{\tilde{T}} \phi_T} \\ m_{\phi_d \phi_{\tilde{T}}} & m_{\phi_u \phi_{\tilde{T}}} & m_{\phi_s \phi_{\tilde{T}}} & m_{\phi_T \phi_{\tilde{T}}} & m_{\phi_{\tilde{T}} \phi_{\tilde{T}}} \end{pmatrix} \quad (\text{A7})$$

where

$$\begin{aligned}
m_{\phi_d\phi_d} &= m_{H_d}^2 + \frac{1}{8}(g_1^2 + g_2^2)(2v_{\bar{T}}^2 - 2v_T^2 + 3v_d^2 - v_u^2) \\
&\quad + \sqrt{2}v_T\Re(T_{\chi_d}) + \frac{|\lambda|^2}{2}(v_s^2 + v_u^2) - v_s v_{\bar{T}}\Re(\chi_d\Lambda_T^*) + (3v_d^2 + 2v_{\bar{T}}^2)|\chi_d|^2, \\
m_{\phi_d\phi_u} &= -\frac{1}{4}(g_1^2 + g_2^2)v_d v_u - \frac{1}{\sqrt{2}}v_s\Re(T_\lambda) + \frac{1}{2}v_T v_{\bar{T}}\Re(\lambda\Lambda_T^*) + v_d v_u |\lambda|^2 \\
&\quad - v_s v_{\bar{T}}\Re(\chi_t\lambda^*) - v_s v_T\Re(\chi_d\lambda^*) - \frac{1}{2}v_s^2\Re(\kappa\lambda^*), \\
m_{\phi_u\phi_u} &= m_{H_u}^2 - \frac{1}{8}(g_1^2 + g_2^2)(2v_{\bar{T}}^2 - 2v_T^2 - 3v_u^2 + v_d^2) \\
&\quad + \sqrt{2}v_{\bar{T}}\Re(T_{\chi_t}) + \frac{1}{2}(v_d^2 + v_s^2)|\lambda|^2 - v_s v_T\Re(\chi_t\Lambda_T^*) + (2v_{\bar{T}}^2 + 3v_u^2)|\chi_t|^2, \\
m_{\phi_d\phi_s} &= v_d v_s |\lambda|^2 - \frac{1}{\sqrt{2}}v_u\Re(T_\lambda) - v_s v_u\Re(\kappa\lambda^*) - v_T v_u\Re(\lambda\chi_d^*) - v_{\bar{T}}v_u\Re(\chi_t\lambda^*) - v_d v_{\bar{T}}\Re(\Lambda_T\chi_d^*), \\
m_{\phi_u\phi_s} &= v_s v_u |\lambda|^2 - \frac{1}{\sqrt{2}}v_d\Re(T_\lambda) - v_d v_s\Re(\lambda\kappa^*) - v_T v_d\Re(\lambda\chi_d^*) - v_d v_{\bar{T}}\Re(\lambda\chi_t^*) - v_T v_u\Re(\chi_t\Lambda_T^*), \\
m_{\phi_s\phi_s} &= m_S^2 + \frac{|\Lambda_T|^2}{2}(v_T^2 + v_{\bar{T}}^2) - v_T v_{\bar{T}}\Re(\kappa\Lambda_T^*) + 3v_s^2|\kappa|^2 - v_d v_u\Re(\lambda\kappa^*) + \frac{1}{2}(v_d^2 + v_u^2)|\lambda|^2, \\
&\quad + \sqrt{2}v_s\Re(T_\kappa), \\
m_{\phi_d\phi_T} &= -\frac{1}{2}(g_1^2 + g_2^2)v_d v_u + \frac{1}{2}v_u v_{\bar{T}}\Re(\lambda\Lambda_T^*) - v_u v_s\Re(\lambda\chi_d^*) + 4v_d v_T |\chi_d|^2 + \sqrt{2}v_d\Re(T_{\chi_d}),
\end{aligned} \tag{A8}$$

$$\begin{aligned}
m_{\phi_u\phi_T} &= \frac{1}{2}(g_1^2 + g_2^2)v_d v_T - v_u v_s\Re(\Lambda_T\chi_t^*) - v_d v_s\Re(\lambda\chi_d^*) + \frac{1}{2}v_d v_{\bar{T}}\Re(\lambda\Lambda_T^*), \\
m_{\phi_s\phi_T} &= v_s v_T |\lambda|^2 - \frac{1}{\sqrt{2}}v_{\bar{T}}\Re(T_\lambda) - v_s v_{\bar{T}}\Re(\kappa\Lambda_T^*) - v_d v_u\Re(\lambda\chi_d^*) - \frac{1}{2}v_u^2\Re(\chi_t\Lambda_T^*), \\
m_{\phi_T\phi_T} &= m_T^2 - \frac{1}{4}(g_1^2 + g_2^2)(2v_{\bar{T}}^2 - 6v_T^2 - v_u^2 + v_d^2) + 2v_d^2|\chi_d|^2 + \frac{1}{2}(v_s^2 + v_{\bar{T}}^2)|\Lambda_T|^2, \\
m_{\phi_d\phi_{\bar{T}}} &= \frac{1}{2}(g_1^2 + g_2^2)v_d v_{\bar{T}} + \frac{1}{2}v_T v_u\Re(\lambda\Lambda_T^*) - v_d v_s\Re(\chi_d\Lambda_T^*) - v_s v_u\Re(\chi_t\lambda^*), \\
m_{\phi_u\phi_{\bar{T}}} &= -\frac{1}{2}(g_1^2 + g_2^2)v_{\bar{T}}v_u + \sqrt{2}v_u\Re(T_{\chi_t}) + \frac{1}{2}v_d v_T\Re(\lambda\Lambda_T^*) - v_d v_s\Re(\lambda\chi_t^*) + 4v_{\bar{T}}v_u |\chi_t|^2, \\
m_{\phi_s\phi_{\bar{T}}} &= v_s v_{\bar{T}} |\Lambda_T|^2 - \frac{1}{\sqrt{2}}v_T\Re(T_\lambda) - v_s v_T\Re(\kappa\Lambda_T^*) - \frac{1}{2}v_d^2\Re(\Lambda_T\chi_d^*) - v_d v_u\Re(\lambda\chi_t^*), \\
m_{\phi_T\phi_{\bar{T}}} &= -(g_1^2 + g_2^2)v_T v_{\bar{T}} - \frac{1}{\sqrt{2}}v_s\Re(T_\lambda) - \frac{1}{2}v_s^2\Re(\kappa\Lambda_T^*) + \frac{1}{2}v_d v_u\Re(\lambda\Lambda_T^*) + v_T v_{\bar{T}} |\Lambda_T|^2, \\
m_{\phi_{\bar{T}}\phi_{\bar{T}}} &= m_{\bar{T}}^2 + \frac{1}{4}(g_1^2 + g_2^2)(v_d^2 - v_u^2 - 2v_T^2 + 6v_{\bar{T}}^2) + \frac{1}{2}(v_s^2 + v_T^2)|\Lambda_T|^2 + 2v_u^2|\chi_t|^2.
\end{aligned} \tag{A9}$$

Appendix B: Constants $C_{abc}^{L,R}$ and factors appeared in our calculation.

Defining $C_{abc}^{L,R}$ in neutron, heavy quarks and mercury EDM calculation, we can find :

$$\begin{aligned}
C_{\bar{q}\bar{q}_i q_j}^L &= -\sqrt{2}g_3 Z_{i,j}^{\bar{q}} e^{i\theta_3}, & C_{\bar{q}\bar{q}_i q_j}^R &= \sqrt{2}g_3 Z_{i,j+3}^{\bar{q}} e^{-i\theta_3}, \\
C_{\bar{q}_j \bar{q}_i \bar{q}}^L &= \sqrt{2}g_3 Z_{i,j+3}^{\bar{q}*} e^{i\theta_3}, & C_{\bar{q}_j \bar{q}_i \bar{q}}^R &= -\sqrt{2}g_3 Z_{i,j}^{\bar{q}*} e^{-i\theta_3}, \\
C_{\bar{\chi}_k^0 \bar{u}_i u_j}^L &= -\frac{1}{6} \left(\sqrt{2}(g_1 Z_{k,1}^{N*} + 3g_2 Z_{k,2}^{N*}) Z_{i,j}^{\bar{u}} + 6Y_{u,j} Z_{k,4}^{N*} Z_{i,j+3}^{\bar{u}} \right), \\
C_{\bar{\chi}_k^0 \bar{u}_i u_j}^R &= -\frac{1}{6} \left(\sqrt{2}(3g_2 Z_{k,2}^N + g_1 Z_{k,1}^N) Z_{i,j}^{\bar{u}*} + 6Y_{u,j}^* Z_{k,4}^N Z_{i,j+3}^{\bar{u}*} \right), \\
C_{\bar{\chi}_k^0 \bar{d}_i d_j}^L &= -\frac{1}{6} \left(\sqrt{2}(g_1 Z_{k,1}^{N*} - 3g_2 Z_{k,2}^{N*}) Z_{i,j}^{\bar{d}} + 6Y_{d,j} Z_{k,3}^{N*} Z_{i,j+3}^{\bar{d}} \right), \\
C_{\bar{\chi}_k^0 \bar{d}_i d_j}^R &= -\frac{1}{6} \left(\sqrt{2}(-3g_2 Z_{k,2}^N + g_1 Z_{k,1}^N) Z_{i,j}^{\bar{d}*} + 6Y_{d,j}^* Z_{k,3}^N Z_{i,j+3}^{\bar{d}*} \right), \\
C_{\bar{d}_j \bar{d}_i \bar{\chi}_k^-}^L &= U_{k,2}^* \sum_{a=1}^3 Y_{d,a} Z_{a,j}^{CKM*} Z_{i,a}^{\bar{u}*}, \\
C_{\bar{d}_j \bar{d}_i \bar{\chi}_k^-}^R &= \sum_{a=1}^3 \left(-g_2 V_{k,1} Z_{a,j}^{CKM} Z_{i,a}^{\bar{u}*} + V_{k,2} Y_{u,a}^* Z_{a,j}^{CKM} Z_{i,a+3}^{\bar{u}*} \right), \\
C_{\bar{\chi}_k^- \bar{d}_i u_j}^L &= \sum_{a=1}^3 \left(-g_2 U_{k,1}^* Z_{j,a}^{CKM*} Z_{i,a}^{\bar{d}} + U_{k,2}^* Y_{d,a} Z_{j,a}^{CKM*} Z_{i,a+3}^{\bar{d}} \right), \\
C_{\bar{\chi}_k^- \bar{d}_i u_j}^R &= V_{k,2} \sum_{a=1}^3 Y_{u,a}^* Z_{j,a}^{CKM} Z_{i,a}^{\bar{d}}, \\
C_{\bar{\chi}_k^- \bar{d}_i u_j}^L &= \sum_{a=1}^3 \left(-g_2 U_{k,1}^* Z_{j,a}^{CKM*} Z_{i,a}^{\bar{d}} + U_{k,2}^* Y_{d,a} Z_{j,a}^{CKM*} Z_{i,a+3}^{\bar{d}} \right), \\
C_{\bar{\chi}_k^- \bar{d}_i u_j}^R &= V_{k,2} \sum_{a=1}^3 Y_{u,a} Z_{j,a}^{CKM} Z_{i,a}^{\bar{d}}, \\
C_{\bar{u}_j \bar{d}_i \bar{\chi}_k^+}^L &= V_{k,2}^* \sum_{a=1}^3 Y_{u,a} Z_{j,a}^{CKM} Z_{i,a}^{\bar{d}}, \\
C_{\bar{u}_j \bar{d}_i \bar{\chi}_k^+}^R &= \sum_{a=1}^3 \left(-g_2 U_{k,1} Z_{j,a}^{CKM} Z_{i,a}^{\bar{d}} + U_{k,2} Y_{d,a} Z_{j,a}^{CKM} Z_{i,a+3}^{\bar{d}} \right), \\
C_{\bar{u}_i h_k u_i} &= -\frac{1}{\sqrt{2}} Y_{u_i} Z_{k,2}^h, \\
C_{\bar{d}_i h_k d_i} &= -\frac{1}{\sqrt{2}} Y_{d_i} Z_{k,1}^h
\end{aligned}$$

(B1)

Defining $C_{abc}^{L,R}$ and $x_i = \frac{m_i^2}{m_W^2}$ in electron EDM calculation, we can find :

$$\begin{aligned}
C_{\bar{e}_i \bar{\nu}_k \tilde{\chi}_j^-}^L &= U_{j,2}^* \sum_{b=1}^3 Z_{kb}^{V,*} \sum_{a=1}^3 U_{R,ia}^{e,*} Y_{e,ab} , \\
C_{\bar{e}_i \bar{\nu}_k \tilde{\chi}_j^-}^R &= -g_2 \sum_{a=1}^3 Z_{ka}^{V,*} U_{L,ia}^e V_{j1} , \\
C_{\tilde{\chi}_j^+ \bar{\nu}_k^* e_j}^L &= -g_2 V_{i1}^* \sum_{a=1}^3 U_{L,ja}^{e,*} Z_{ka}^V , \\
C_{\tilde{\chi}_j^+ \bar{\nu}_k^* e_j}^R &= \sum_{b=1}^3 \sum_{a=1}^3 Y_{e,ab}^* U_{R,ja}^e Z_{kb}^V U_{i2} , \\
C_{\tilde{\chi}_i^0 \bar{e}_k^* e_j}^L &= \frac{1}{2} (-2N_{i3}^* \sum_{b=1}^3 U_{L,jb}^{e,*} \sum_{a=1}^3 Y_{e,ab} Z_{k3+a}^E + \sqrt{2}g_1 N_{i1}^* \sum_{a=1}^3 U_{L,ja}^{e,*} Z_{ka}^E \\
&\quad + \sqrt{2}g_2 N_{i2}^* \sum_{a=1}^3 U_{L,ja}^{e,*} Z_{ka}^E) , \\
C_{\tilde{\chi}_i^0 \bar{e}_k^* e_j}^R &= -\sqrt{2}g_1 \sum_{a=1}^3 Z_{k3+a}^E U_{R,ja}^e N_{i1} - \sum_{b=1}^3 \sum_{a=1}^3 Y_{e,ab}^* U_{R,ja}^e Z_{kb}^E N_{i3} , \\
C_{\bar{e}_i \bar{e}_k \tilde{\chi}_j^0}^L &= -2N_{j3}^* \sum_{b=1}^3 Z_{kb}^{E,*} \sum_{a=1}^3 U_{R,ia}^{e,*} Y_{e,ab} - \sqrt{2}g_1 N_{j1}^* \sum_{a=1}^3 Z_{k3+a}^{E,*} U_{R,ia}^{e,*} , \\
C_{\bar{e}_i \bar{e}_k \tilde{\chi}_j^0}^R &= \frac{1}{2} (-2 \sum_{b=1}^3 \sum_{a=1}^3 Y_{e,ab}^{e,*} Z_{k3+a}^{E,*} U_{L,ib}^e N_{j3} + \sqrt{2} \sum_{a=1}^3 Z_{ka}^{E,*} U_{L,ia}^e (g_1 N_{j1} + g_2 N_{j2}))
\end{aligned} \tag{B2}$$

The functions $I_{1,2,3}(x)$ in III A and $I_{1,2,3}(x_1, x_2)$ in III C can be written as

$$\begin{aligned}
I_1(x) &= \frac{1}{2(x-1)^2} \left(1 + x + \frac{2x}{x-1} \ln x \right), \\
I_2(x) &= \frac{1}{6(x-1)^2} \left(10x - 26 - \frac{2x-18}{x-1} \ln x \right), \\
I_3(x) &= \frac{1}{2(x-1)^2} \left(3 - x + \frac{2}{x-1} \ln x \right), \\
I_1(x_1, x_2) &= \frac{1}{16\pi^2} \left[\frac{1 + \ln x_2}{(x_2 - x_1)} + \frac{x_1 \ln x_1 - x_2 \ln x_2}{(x_2 - x_1)^2} \right],
\end{aligned} \tag{B3}$$

$$\begin{aligned}
I_2(x_1, x_2) &= \frac{1}{16\pi^2} \left[-\frac{1 + \ln x_1}{(x_2 - x_1)} - \frac{x_1 \ln x_1 - x_2 \ln x_2}{(x_2 - x_1)^2} \right], \\
I_3(x_1, x_2) &= \frac{1}{32\pi^2} \left[\frac{3 + 2 \ln x_2}{(x_2 - x_1)} - \frac{2x_2 + 4x_2 \ln x_2}{(x_2 - x_1)^2} - \frac{2x_1^2 \ln x_1}{(x_2 - x_1)^3} \right. \\
&\quad \left. + \frac{2x_2^2 \ln x_2}{(x_2 - x_1)^3} \right], \\
I_4(x_1, x_2) &= \frac{1}{96\pi^2} \left[\frac{11 + 6 \ln x_2}{(x_2 - x_1)} - \frac{15x_2 + 18x_2 \ln x_2}{(x_2 - x_1)^2} + \frac{6x_2^2 + 18x_2^2 \ln x_2}{(x_2 - x_1)^3} \right. \\
&\quad \left. + \frac{6x_1^3 \ln x_1 - 6x_2^3 \ln x_2}{(x_2 - x_1)^4} \right].
\end{aligned} \tag{B4}$$

Appendix C: Effective Lagrangian in our calculation.

The $\bar{q}\tilde{q}_i g$ interaction is given by [53]

$$\mathcal{L}_{eff} = -\sqrt{2}g_s \sum_a T^a \left\{ \bar{u}_L V_u^{LL} u_L - \bar{u}_R V_u^{RR} u_R + \bar{d}_L V_d^{LL} d_L - \bar{d}_R V_d^{RR} d_R \right\} + H.c. \tag{C1}$$

The $\bar{q}\tilde{q}_i \chi_j^+$ interaction is given by [54]

$$\begin{aligned}
\mathcal{L}_{eff} &= g\bar{t}((R_{bij} + \Delta R_{bij})P_R + (L_{bij} + \Delta L_{bij})P_L)\tilde{\chi}_j^+ \tilde{b}_i \\
&+ g\bar{b}((R_{tij} + \Delta R_{tij})P_R + (L_{tij} + \Delta L_{tij})P_L)\tilde{\chi}_j^c \tilde{t}_i + H.c.
\end{aligned} \tag{C2}$$

The $\bar{q}\tilde{q}_i \chi_j^0$ interaction is given by [54]

$$\begin{aligned}
\mathcal{L}_{eff} &= g\bar{b}[(K_{bij} + \Delta K_{bij})P_R + (M_{bij} + \Delta M_{bij})P_L]\chi_j^0 \tilde{b}_i \\
&+ g\bar{t}[(K_{tij} + \Delta K_{tij})P_R + (M_{tij} + \Delta M_{tij})P_L]\chi_j^0 \tilde{t}_i + H.c.
\end{aligned} \tag{C3}$$

-
- [1] K. Abe *et al.* [Belle Collaboration], Phys. Rev. Lett. **87**, 091802 (2001).
 - [2] T. Modak and E. Senaha, Phys. Lett. B **822** (2021), 136695
 - [3] B. Aubert *et al.* [BaBar Collaboration], Phys. Rev. Lett. **89**, 201802 (2002).
 - [4] M. Dine and A. Kusenko, *Reviews of Modern Physics* **76**, 1 (2003).

- [5] T. Modak and E. Senaha, *JHEP* **11** (2020), 025
- [6] M. Masip, *Phys. Lett. B* **444** (1998), 352-357
- [7] J. L. Yang, T. F. Feng, S. K. Cui, C. X. Liu, W. Li and H. B. Zhang, *JHEP* **04**, 013 (2020).
- [8] J. R. Ellis, S. Ferrara and D. V. Nanopoulos, *Phys. Lett.* 114B, 231 (1982).
- [9] J. Polchinski and M. B. Wise, *Phys. Lett.* **125B**, 393 (1983).
- [10] P. Nath, *Phys. Rev. Lett.* **66**, 2565 (1991).
- [11] Y. Kizukuri and N. Oshimo, *Phys. Rev. D* **46**, 3025 (1992).
- [12] Y. Kizukuri and N. Oshimo, *Phys. Rev. D* **45**, 1806 (1992).
- [13] P. Bandyopadhyay, K. Huitu and A. Sabanci, *JHEP* 1310 (2013) 091 [arXiv:1306.4530 [hep-ph]].
- [14] P. Bandyopadhyay, S. Di Chiara, K. Huitu and A. S. Keceli, *JHEP* 1411 (2014) 062
- [15] S. F. King, M. Muhlleitner, R. Nevzorov and K. Walz, *Nucl. Phys. B* **901** (2015), 526-555
- [16] Particle Data Group, *Review of Particle Physics*, **83C**, 1 (2023).
- [17] J. Baron et al, (ACME Collaboration), *Science* **343**, 269 (2014).
- [18] V. Andreev et al, (ACME Collaboration), *Nature* **562**, 355-360 (2018).
- [19] A. E. Blinov and A. S. Rudenko, *Nucl. Phys. Proc. Suppl.* **189**, 257 (2009).
- [20] S. Navas et al. (Particle Data Group), *Phys. Rev. D* 110, 030001 (2024).
- [21] B. Graner, Y. Chen, E. G. Lindahl and B. R. Heckel, *Phys. Rev. Lett.* **116**, no.16, 161601 (2016) [erratum: *Phys. Rev. Lett.* **119**, no.11, 119901 (2017)]
- [22] F. Sala, *JHEP* **1403**, 061 (2014).
- [23] M. Pospelov and A. Ritz, *Phys. Rev. D* **63**, 073015 (2001).
- [24] E. Braaten, C. S. Li and T. C. Yuan, *Phys. Rev. Lett.* **64**, 1709 (1990).
- [25] G. Degrassi, E. Franco, S. Marchetti and L. Silvestrini, *JHEP* **0511**, 044 (2005).
- [26] H. Gisbert and J. Ruiz Vidal, arXiv:1905.02513 [hep-ph].
- [27] D. Chang, W. Y. Keung, C. S. Li and T. C. Yuan, *Phys. Lett. B* **241**, 589 (1990).
- [28] J. R. Espinosa and M. Quiros, *Phys. Lett. B* **302** (1993), 51-58
- [29] J. R. Espinosa and M. Quiros, *Phys. Rev. Lett.* **81** (1998), 516-519
- [30] K. Agashe, A. Azatov, A. Katz and D. Kim, *Phys. Rev. D*, **84**, 115024 (2011).
- [31] U. Ellwanger, C. Hugonie, and A. M. Teixeira, *Phys. Rep.* **496**, 1 (2010).

- [32] S. Chang, R. Dermisek, J. F. Gunion, and N. Weiner, *Annu. Rev. Nucl. Part. Sci.* **58**, 75 (2008).
- [33] J. R. Espinosa, *PoS TOP2015* (2016), 043
- [34] J. R. Espinosa, T. Konstandin and F. Riva, *Nucl. Phys. B* **854** (2012), 592-630.
- [35] J. Elias-Miro, J. R. Espinosa, G. F. Giudice, G. Isidori, A. Riotto and A. Strumia, *Phys. Lett. B* **709** (2012), 222-228.
- [36] T. Falk and K. A. Olive, *Phys. Lett. B* **375**, 196 (1996).
- [37] T. Falk and K. A. Olive, *Phys. Lett. B* **439**, 71 (1998).
- [38] M. Brhlik, G. J. Good and G. L. Kane, *Phys. Rev. D* **59**, 115004 (1999).
- [39] A. Bartl, T. Gajdosik, W. Porod, P. Stockinger and H. Stremnitzer, *Phys. Rev. D* **60**, 073003 (1999).
- [40] S. Abel, S. Khalil and O. Lebedev, *Nucl. Phys. B* **606**, 151 (2001) [[hep-ph/0103320](#)].
- [41] V. D. Barger, T. Falk, T. Han, J. Jiang, T. Li and T. Plehn, *Phys. Rev. D* **64**, 056007 (2001) [[hep-ph/0101106](#)].
- [42] K. A. Olive, M. Pospelov, A. Ritz and Y. Santoso, *Phys. Rev. D* **72**, 075001 (2005) [[hep-ph/0506106](#)].
- [43] V. Cirigliano, S. Profumo and M. J. Ramsey-Musolf, *JHEP* **0607**, 002 (2006) [[hep-ph/0603246](#)].
- [44] S. Y. Ayazi and Y. Farzan, *Phys. Rev. D* **74**, 055008 (2006)
- [45] V. Barger, P. Fileviez Perez and S. Spinner, *Phys. Rev. Lett* **102**, 181802 (2009) [[arXiv:0812.3661 \[hep-ph\]](#)].
- [46] P. Fileviez Perez and S. Spinner, *Phys. Lett. B* **673**, 251 (2009) [[arXiv:0811.3424 \[hep-ph\]](#)].
- [47] H. X. Chen, S. K. Cui, N. Y. Zhu, Z. Y. Zhang and H. C. Hu, *Chin. Phys. C* **48** (2024) no.5, 053104.
- [48] H. c. Hu, Z. Y. Zhang, N. Y. Zhu and H. X. Chen, *Chin. Phys. C* **48** (2024) no.9, 093101.
- [49] Z. Y. Zhang, J. L. Yang, H. B. Zhang and T. F. Feng, *Phys. Rev. D* **110** (2024) no.1, 015035.
- [50] J. Dai, H. Dykstra, R. G. Leigh, S. Paban and D. Dicus, *Phys. Lett. B*
- [51] D. A. Dicus, *Phys. Rev. D* **41**, 999 (1990).
- [52] T. F. Feng, X. Q. Li, J. Maalampi and X. M. Zhang, *Phys. Rev. D* **71**, 056005 (2005) [[arXiv:](#)

- 0412147].
- [53] J. Cao, D. Li, L. Shang, P. Wu and Y. Zhang, JHEP **12** (2014), 026.
 - [54] T. Ibrahim and P. Nath, Phys. Rev. D **71** (2005), 055007.
 - [55] R. L. Arnowitt, J. L. Lopez and D. V. Nanopoulos, Phys. Rev. D **42**, 2423-2426 (1990).
 - [56] R. L. Arnowitt, M. J. Duff and K. S. Stelle, Phys. Rev. D **43**, 3085-3088 (1991).
 - [57] F. Staub, arXiv:0806.0538.
 - [58] F. Staub, Comput.Phys.Commun. **181** 1077-1086 (2010) [arXiv:0909.2863].
 - [59] F. Staub, Comput.Phys.Commun. **182** 808-833 (2011) [arXiv:1002.0840].
 - [60] F. Staub, Comput.Phys.Commun. **184** 1792-1809 (2013) [arXiv:1207.0906].
 - [61] F. Staub, Comput.Phys.Commun. **185** 1773-1790 (2014) [arXiv:1309.7223].
 - [62] T. F. Feng, X. Q. Li, J. Maalampi and X. M. Zhang, Phys. Rev. D **71**, 056005 (2005).
 - [63] G. F. Giudice and A. Romanino, Phys. Lett. B **634**, 307 (2006).
 - [64] B. Yan, S. M. Zhao, and T. F. Feng *et al.* [Authors], *Nucl. Phys. B*
 - [65] C. Lee, V. Cirigliano and M. J. Ramsey-Musolf, Phys. Rev. D **71**, 075010 (2005)
 - [66] H. B. Zhang, T. F. Feng, S. M. Zhao and T. J. Gao, Nucl. Phys. B **873**, 300 (2013) [Erratum: Nucl. Phys. B **879**, 235 (2014)].
 - [67] H. B. Zhang, T. F. Feng, G. H. Luo, Z. F. Ge and S. M. Zhao, JHEP **1307**, 069 (2013) [Erratum: JHEP **1310**, 173 (2013)].
 - [68] R. L. Workman *et al.* (PDG), Prog. Theor. Exp. Phys. **2022**, 083C01 (2022).
 - [69] CMS Collab., Phys. Lett. B, **716**, 30 (2012).
 - [70] ATLAS Collab., Phys. Lett. B, **716**, 1 (2012).
 - [71] P.Cox, C.C. Han, T.T. Yanagida, Phys. Rev. D **104** 075035 (2021).
 - [72] M. V. Beekveld, W. Beenakker, M. Schutten, et al., SciPost Phys. **11** 3 (2021) [arXiv:2104.03245 [hep-ph]].
 - [73] M. Chakraborti, L. Roszkowski, S. Trojanowski, JHEP **05** 252 (2021) [arXiv:2104.04458 [hep-ph]].
 - [74] F. Wang, L. Wu, Y. Xiao, et al., Nucl. Phys. B **970**, 115486 (2021) [arXiv:2104.03262 [hep-ph]].
 - [75] M. Chakraborti, S. Heinemeyer, I. Saha, Eur. Phys. J. C **81** 12 (2021) [arXiv:2104.03287 [hep-ph]].

- [76] M. Endo, K. Hamaguchi, S. Iwamoto, et al., JHEP **07** 075 (2021) [arXiv:2104.03217 [hep-ph]].
975 (2022) 115671,doi: 10.1016/j.nuclphysb.2022.115671,[arXiv:2011.0853 [hep-ph]].
- [77] K. Agashe, A. Azatov, A. Katz and D. Kim,Phys. Rev. D **84** (2011),115024.
- [78] Z. J. Yang, J. L. Yang, S. M. Zhao, X. G. Wu and T. F. Feng, [arXiv:2410.13659 [hep-ph]].
- [79] G. Aad *et al.* [ATLAS],JHEP **10**, 062 (2020)[arXiv:2008.06032].
- [80] C. S. Un and O. Ozdal, Phys. Rev. D **93**, 055024 (2016).
- [81] K. Cheung, T. J. Hou, J. S. Lee and E. Senaha,Phys. Rev. D **84** (2011), 015002.
- [82] J. Ruiz Vidal,[arXiv:2407.19247 [hep-ph]].